Direct measurements of low-energy resonance strengths of the ^{23}Na(p,γ)^{24}Mg reaction for astrophysics

A. Boeltzig [a,b,c,d,*], A. Best [e,f], F.R. Pantaleo [g,h], G. Imbriani [e,f], M. Junker [d,a], M. Aliotta [i],
J. Balibrea-Correa [e,f], D. Bemmerer [j], C. Broggini [l], C.G. Bruno [i], R. Buompane [f,k],
A. Caciolli [m,l], F. Cavanna [n], T. Chillery [i], G.F. Ciani [a,d], P. Corvisiero [o,n], L. Csedreki [d,a],
T. Davinson [i], R.J. deBoer [b,c], R. Depalo [m,l], A. Di Leva [e,f], Z. Elekes [p], F. Ferraro [o,n],
E.M. Fiore [g,h], A. Formicola [d], Zs. Fülöp [p], G. Gervino [q,r], A. Guglielmetti [s,t], C. Gustavino [u],
Gy. Gyürky [p], I. Kochanek [d], M. Lugaro [v], P. Marigo [l,m], R. Menegazzo [l], V. Mossa [g,h],
F. Munnik [j], V. Paticchio [h], R. Perrino [h,1], D. Piatti [m,l], P. Prati [o,n], L. Schiavulli [g,h],
K. Stöckel [j,w], O. Straniero [x,d], F. Strieder [y], T. Szücs [j], M.P. Takács [j,w,2], D. Trezzi [s,t],
M. Wiescher [b,c], S. Zavatarelli [n]

[a] Gran Sasso Science Institute, Viale F. Crispi 7, 67100 L'Aquila, Italy
[b] The Joint Institute for Nuclear Astrophysics, University of Notre Dame, Notre Dame, IN 46556, USA
[c] Department of Physics, University of Notre Dame, Nieuwland Science Hall 225, Notre Dame, IN 46556-5670, USA
[d] Istituto Nazionale di Fisica Nucleare, Laboratori Nazionali del Gran Sasso (LNGS), Via G. Acitelli 22, 67100 Assergi, Italy
[e] Università degli Studi di Napoli "Federico II", Dipartimento di Fisica "E. Pancini", Via Cinthia 21, 80126 Napoli, Italy
[f] Istituto Nazionale di Fisica Nucleare, Sezione di Napoli, Via Cintia 21, 80126 Napoli, Italy
[g] Università degli Studi di Bari, Dipartimento Interateneo di Fisica, Via G. Amendola 173, 70126 Bari, Italy
[h] Istituto Nazionale di Fisica Nucleare, Sezione di Bari, Via E. Orabona 4, 70125 Bari, Italy
[i] School of Physics and Astronomy, University of Edinburgh, Peter Guthrie Tait Road, EH9 3FD Edinburgh, United Kingdom
[j] Helmholtz-Zentrum Dresden-Rossendorf, Bautzner Landstraße 400, 01328 Dresden, Germany
[k] Università degli Studi della Campania "L. Vanvitelli", Dipartimento di Matematica e Fisica, Viale Lincoln 5, 81100 Caserta, Italy
[l] Istituto Nazionale di Fisica Nucleare, Sezione di Padova, Via F. Marzolo 8, 35131 Padova, Italy
[m] Università degli Studi di Padova, Via F. Marzolo 8, 35131 Padova, Italy
[n] Istituto Nazionale di Fisica Nucleare, Sezione di Genova, Via Dodecaneso 33, 16146 Genova, Italy
[o] Università degli Studi di Genova, Via Dodecaneso 33, 16146 Genova, Italy
[p] Institute for Nuclear Research of the Hungarian Academy of Sciences (MTA Atomki), PO Box 51, 4001 Debrecen, Hungary
[q] Università degli Studi di Torino, Via P. Giuria 1, 10125 Torino, Italy
[r] Istituto Nazionale di Fisica Nucleare, Sezione di Torino, Via P. Giuria 1, 10125 Torino, Italy
[s] Università degli Studi di Milano, Via G. Celoria 16, 20133 Milano, Italy
[t] Istituto Nazionale di Fisica Nucleare, Sezione di Milano, Via G. Celoria 16, 20133 Milano, Italy
[u] Istituto Nazionale di Fisica Nucleare, Sezione di Roma, Piazzale A. Moro 2, 00185 Roma, Italy
[v] Konkoly Observatory, Research Centre for Astronomy and Earth Sciences, Hungarian Academy of Sciences, 1121 Budapest, Hungary
[w] Technische Universität Dresden, Institut für Kern- und Teilchenphysik, Zellescher Weg 19, 01069 Dresden, Germany
[x] INAF – Osservatorio Astronomico d'Abruzzo, Via Mentore Maggini, 64100 Teramo, Italy
[y] Department of Physics, South Dakota School of Mines and Technology, 501E St Joseph Street, Rapid City, SD 57701, USA

A R T I C L E   I N F O

A B S T R A C T

The NeNa and the MgAl cycles play a fundamental role in the nucleosynthesis of asymptotic giant branch stars undergoing hot bottom burning. The ^{23}Na(p, γ)^{24}Mg reaction links these two cycles and a precise determination of its rate is required to correctly estimate the contribution of these stars to the chemical evolution of various isotopes of Na, Mg and Al. At temperatures of $50 \lesssim T \lesssim 110$ MK, narrow resonances at $E_p = 140$ and 251 keV are the main contributors to the reaction rate, in addition to the direct capture that dominates in the lower part of the temperature range. We present new measurements of the strengths of these resonances at the Laboratory for Underground Nuclear Astrophysics (LUNA).

* Corresponding author at: Istituto Nazionale di Fisica Nucleare, Laboratori Nazionali del Gran Sasso (LNGS), Via G. Acitelli 22, 67100 Assergi, Italy.
  E-mail address: axel.boeltzig@gssi.infn.it (A. Boeltzig).
[1] Permanent address: Istituto Nazionale di Fisica Nucleare, Sezione di Lecce, Via Arnesano, 73100 Lecce, Italy.
[2] Current address: Physikalisch-Technische Bundesanstalt, Bundesallee 100, 38116 Braunschweig, Germany.

We have used two complementary detection approaches: high efficiency with a 4π BGO detector for the 140 keV resonance, and high resolution with a HPGe detector for the 251 keV resonance. Thanks to the reduced cosmic ray background of LUNA, we were able to determine the resonance strength of the 251 keV resonance as $\omega\gamma = 482(82)\,\mu\text{eV}$ and observed new gamma ray transitions for the decay of the corresponding state in ^{24}Mg at $E_x = 11931$ keV. With the highly efficient BGO detector, we observed a signal for the 140 keV resonance for the first time in a direct measurement, resulting in a strength of $\omega\gamma_{140} = 1.46^{+0.58}_{-0.53}$ neV (68% CL). Our measurement reduces the uncertainty of the $^{23}\text{Na}(\text{p},\gamma)^{24}\text{Mg}$ reaction rate in the temperature range from 0.05 to 0.1 GK to at most $^{+50\%}_{-35\%}$ at 0.07 GK. Accordingly, our results imply a significant reduction of the uncertainties in the nucleosynthesis calculations.
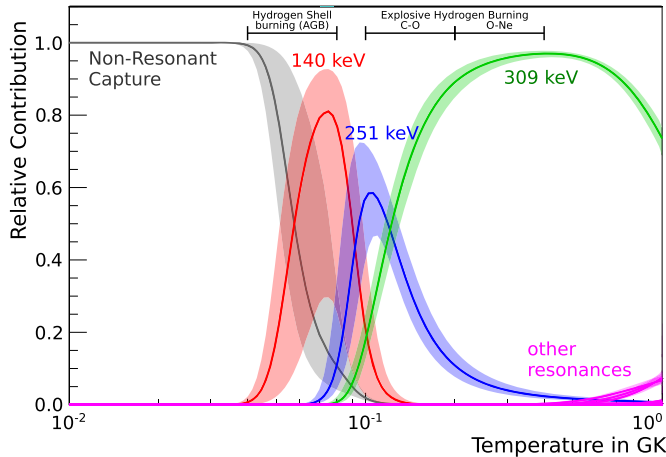
Fig. 1. Fractional contributions of the narrow resonances and the non-resonant cross section to the reaction rate at different stellar temperatures. The bands result from sampling the resonance parameters according to the parameters and procedures in [9–11].

Table 1

Nuclear resonance parameters for the $^{23}\text{Na}(\text{p},\gamma)^{24}\text{Mg}$ reaction rate calculation as used in [9] and shown in Fig. 1. The upper limit for $\omega\gamma_{140\,\text{keV}}$ corresponds to 95% CL.

	140 keV	251 keV	309 keV
E_x (keV)	[18,19], [17] 11827(4), 11830.7(15)	[18,19] 11931.2(6)	[18,19] 11987.72(10)
E_p (keV)	[18,19], [17,9] 140.2(42), 144.0(16)	[16] 250.9(2)	[16] 308.75(6)
Γ_{tot} (keV)		[16,20] < 0.02	[16,21] < 0.002
$\omega\gamma$ (eV)	[9] $< 5.17 \times 10^{-9}$	[12,16] $5.25(175) \times 10^{-4}$	[12,16] $1.05(19) \times 10^{-1}$

figure use the current best upper limit for the strength of the 140 keV resonance quoted in the literature [9] and treated as in [11]. Strengths of the 251 keV and 309 keV resonances have been measured by [12–15]; and the calculations presented in Fig. 1 use the values as compiled in [16]. Information on the direct capture cross section was used as obtained indirectly in [17]. The nuclear properties of the resonances are summarized in Table 1.

The upper limit on the strength of the 140 keV resonance [9] does not exclude this resonance from being the dominant contribution to the reaction rate at $T \sim 80 - 90$ MK. In fact, the uncertainty of the $^{23}\text{Na}(\text{p},\gamma)^{24}\text{Mg}$ reaction rate in the discussed temperature range, associated with the upper limit of the 140 keV resonance strength and the 33% relative uncertainty of the 251 keV resonance strength, provide a strong motivation for an experimental study of these resonances.

1. Introduction

Asymptotic Giant Branch (AGB) stars provide a major contribution to the synthesis of the elements in the cosmos and specifically to the chemical evolution of stellar clusters and galaxies. The more massive AGB stars ($M \gtrsim 4\,M_\odot$) undergo proton captures at the base of the convective envelope (hot bottom burning, HBB) [1,2]. When the convective envelope extends down to the H-burning shell, the ashes of the CNO, NeNa and MgAl cycles appear at the stellar surface. The coupling between convection and nuclear burning is responsible for the synthesis of various isotopes of Na, Mg and Al.

Combined, the uncertainties of the $^{23}\text{Na}(\text{p},\gamma)^{24}\text{Mg}$ and the $^{22}\text{Ne}(\text{p},\gamma)^{23}\text{Na}$ reaction rates account for the major nuclear contribution to the uncertainty of predicted ^{23}Na and ^{24}Mg yields from these massive AGB stars [3]. The $^{23}\text{Na}(\text{p},\gamma)^{24}\text{Mg}$ reaction, in particular, is the bridge between the NeNa and MgAl cycles. The $^{22}\text{Ne}(\text{p},\gamma)^{23}\text{Na}$ reaction has been subject of recent experimental studies [4–8]; prior studies of $^{23}\text{Na}(\text{p},\gamma)^{24}\text{Mg}$ are described below.

During HBB, the temperatures at the bottom of the convective envelopes range between $50 \lesssim T \lesssim 110$ MK, increasing with the stellar mass and decreasing with the metallicity. The $^{23}\text{Na}(\text{p},\gamma)^{24}\text{Mg}$ reaction rate in this temperature range is dominated by two resonances at $E_p = 140$ and 251 keV, where E_p is the proton beam energy in the laboratory system throughout this paper. At lower energies, the non-resonant capture contribution dominates the reaction rate, whereas another narrow resonance at $E_p = 309$ keV is the principal component of the reaction rate at higher temperatures, up to $T = 1$ GK. The relative importance of each contribution for the reaction rate at different temperatures is illustrated in Fig. 1. The reaction rate calculations shown in this

2. Methodology

2.1. Setup

The measurements were performed at the Laboratory for Underground Nuclear Astrophysics (LUNA), located at the Gran Sasso National Laboratory. Proton beams with energies of 130 to 400 keV were provided by the LUNA400 accelerator [22] and used to bombard water-cooled solid targets. Typical beam intensities of 100-250 μA on target were obtained.

Two complementary setups were used to study the cross section: one employed a High-Purity Germanium (HPGe) detector, the other a segmented Bismuth Germanium Oxide (BGO) summing detector. The use of two setups is advisable, as the efficiency of the HPGe detector is too low to study the weak 140 keV resonance. The energy resolution of the HPGe detector, however, significantly facilitates the study the gamma-ray branchings of the stronger resonances at 251 keV and 309 keV.

Both setups benefit from the underground location of LUNA at the Gran Sasso National Laboratory, and target and detectors were surrounded by a massive lead shielding to reduce background from environmental radiation [23–25].

2.2. BGO detector phase: 140 keV resonance

The segmented BGO summing detector was used to search for the 140 keV resonance with a large detection efficiency, utilizing a digital data acquisition system to acquire independent spectra of the six individual crystals and generating a sum energy spectrum offline [25,26, and references therein]. The response of the BGO detector was estimated through a Monte Carlo simulation using Geant4 [27,26], which was validated with calibration measurements. The efficiency for the detection of the full gamma-ray energy depends on the gamma-ray branching ratios and the low-energy threshold of the individual crystal segment. In the case of the 309 keV resonance, for example, the detection efficiency above 10 MeV is about 50% [25]; the efficiency of this detector is further discussed in subsection 3.2. In the search for the $E_p = 140$ keV resonance, measurements were taken at beam energies around 130, 140, 145 and 147 keV, in view of the uncertainty of the resonance energy (see Table 1). Due to a narrow resonance in $^{18}O(p, \gamma)^{19}F$ ($Q = 7994$ keV) at $E_p = 151$ keV, the background from random coincidence summing (pile-up) of gamma rays from this reaction prohibited the $^{23}Na(p, \gamma)^{24}Mg$ resonance search for beam energies above 151 keV. At energies of 140 keV and below we observed yields compatible with zero within the statistical uncertainty. For the runs at 147 keV (147 keV $\lesssim E_p \lesssim 149$ keV) we observe a statistically significant excess of counts over the beam-induced background. This beam energy is compatible with the resonance energy in literature, and we analyzed this data set considering these runs as on-resonance, taking into account the target thickness (described in sec. 2.4).

2.3. HPGe detector phase: 251 keV and 309 keV resonances

The HPGe detector was employed in close geometry at an angle of 55° to study the resonance strengths and gamma-ray branchings of the resonances at 251 keV and 309 keV (cf. [28, and references therein]). The efficiency calibration was based on radioactive sources (^{137}Cs, ^{60}Co) and gamma rays from narrow resonances at $E_p = 326$ keV in $^{27}Al(p, \gamma)^{28}Si$ and at $E_p = 278$ keV in $^{14}N(p, \gamma)^{15}O$. An empirical calibration curve was fitted to the total and full energy peak efficiency, using the parametrization in [29]. Summing effects that arise from the coincident detection of multiple gamma rays of the same cascade (enhanced by the close detector geometry) were taken into account, based on the parametrized efficiency curve; angular correlations were neglected for the calculation of the summing effects. The parameters of the efficiency model were determined in a global maximum likelihood fit. We considered an uncertainty of 8% for the efficiency calibration curve, taking into account the scatter of the calibration data points, the repeatability of the (p, γ) calibration measurements, and the few available sources to calibrate the efficiency at gamma energies above 8 MeV.

2.4. Targets

All targets were produced by evaporation of sodium compounds onto a high purity tantalum backing at the Institute for Nuclear Research, Hungarian Academy of Sciences (MTA Atomki). The backing was chemically cleaned and heated in vacuum before the evaporation. We tested several sodium compounds (NaCl, Na_2SiO_3, Na_2WO_4), and obtained the best results (i.e., reproducible target
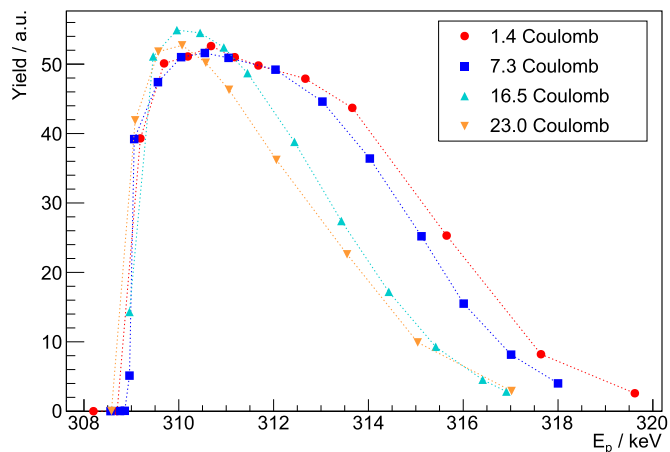

Fig. 2. Yield curves showing scans of the narrow resonance at 309 keV for the same target after different amounts of charge accumulated on this target.

properties and stability under beam) with Na_2WO_4 (as in [9]). In a test evaporation of Na_2WO_4 onto a carbon backing we observed no major deviations in the stoichiometry of the sodium compound with respect to the nominal composition in a Rutherford backscattering measurement. Materials supplied by different vendors were tested in an effort to reduce beam-induced backgrounds from light contaminants, and the cleanest material was chosen for target production.

Typical target thicknesses for the Na_2WO_4 targets were 50 μg/cm² (beam energy loss of about 14 keV at 150 keV proton energy). Between experimental runs we regularly performed measurements of the target thickness by means of nuclear resonance analysis, scanning over the 309 keV resonance in $^{23}Na(p, \gamma)^{24}Mg$. Targets were replaced when the target thickness (width of the plateau in a 309 keV resonance scan) had decreased strongly, or a drop in on-resonance yield was observed. An example for the development of the target scan under bombardment is shown in Fig. 2. Typical accumulated charges on a single target ranged between 10 and 30 C.

Elastic Recoil Detection Analysis (ERDA) was performed on selected targets at the Ion Beam Center at the Helmholtz-Center Dresden-Rossendorf, using a 43 MeV Cl^{7+} beam and detecting the recoils at an angle of 31° (cf. [30] for a description of the setup). Analysis of the data with the program NDF [31] resulted in depth profile information and allowed for the study of the chemical composition of various targets during the initial target development phase. Furthermore, two targets were produced under identical conditions: one was used to measure the 251 keV and 309 keV resonances with the HPGe detector setup at LUNA, the other was not bombarded. Both of these targets were also analyzed with ERDA to study the chemical composition for the analysis of the HPGe measurements. Depth profiles were obtained and the stoichiometry of Na, W, O and H in the main target layer resulted in effective stopping powers that were on the order of 10% larger compared to the nominal composition of pure Na_2WO_4. Traces of carbon were detected in the bulk of the samples, but the amount was irrelevant in the context of our measurement.

3. Analysis and results

3.1. HPGe detector phase: 251 keV and 309 keV resonances

With the effective stopping power of the material at the resonance energy, ε_{eff}, the absolute strength $\omega\gamma$ of the narrow resonances can be determined through the well-known relation

$Y = \frac{\lambda^2}{2} \frac{\omega\gamma}{\varepsilon_{\text{eff}}}$ [32], where Y is the reaction yield (number of re-actions per incident projectile), and λ the de Broglie wavelength of the projectile. Stopping power tables were generated using SRIM 2013.00 [33].

Branching ratios and resonance strengths were determined solving the system of equations: $N_i = \sum_j \left(B_{ij} \cdot P_j \right) \cdot Y \cdot \frac{Q}{q_p}$, where the vector elements N_i are the number of counts in the primary gamma-ray peaks, and the matrix elements B_{ij} correspond to the probability that a decay through the primary branch i is registered in the primary peak j (including detection efficiency and summing effects). The vector elements P_i are the primary branching ratios that fulfill the normalization condition $\sum P_i = 1$ and Q and q_p are the accumulated charge on target and the charge of a single projectile (proton), respectively.

When calculating the summing effects, gamma-ray branch-ing ratios for secondary transitions were taken from literature [18]. The uncertainties of Y and the P_i were determined by a Monte Carlo approach, repeating the analysis after varying the N_i within the respective experimental uncertainties and the sec-ondary branching ratios within their uncertainties given in litera-ture. The uncertainty of ε_{eff}, derived from the uncertainty of the chemical composition of the target as determined with ERDA, typ-ically amounted to 15% and was the dominant contribution to the resonance strength uncertainty. A systematic uncertainty of 3% was assumed for the measurement of the accumulated charge on tar-get.

Among the ^{23}Na(p, γ)^{24}Mg resonances in Table 1, the strength of that at $E_p = 309$ keV is the best known in literature [16]. To verify our results, we redetermined the resonance strength and gamma-ray branching ratios as described above. The branching ra-tios of the 12 primary transitions in literature [18] were found to be in agreement with our measurement within the experi-mental uncertainties. The height of the plateau of two resonance scans on target and the composition of the not bombarded tar-get as determined by ERDA resulted in a resonance strength of $\omega\gamma_{309} = 108(19)$ meV, in good agreement with the literature value of $105(19)$ meV [16].

The strength of the resonance at $E_p = 251$ keV is known with a larger uncertainty of about 33% (Table 1). Additionally, the gamma-ray branchings of the corresponding level in ^{24}Mg are not given in current compilations (such as [19]), and the only publication of these branching ratios known to the authors indicates only two strong transitions from this level [34]. A scan of the 251 keV res-onance, followed by a long run ($Q \approx 11$ C) at an energy on the resonance, was used to determine the strength of this resonance and the gamma-ray branching ratios of the corresponding level in ^{24}Mg. The most intense transitions are marked in the spectrum in Fig. 3 and the resulting branching ratios are given in Table 2. In addition to the two major transitions described in [34], we identified multiple minor transitions and determined their branch-ing ratios. The intensities of several minor peaks in the spectrum, most prominently the transition to the ground state of ^{24}Mg, were consistent with the expectation from true coincidence summing (summing-in) alone and are thus not included in Table 2.

With the yield of the long run on the resonance plateau and using the same target stoichiometry as in the analysis of the 309 keV resonance, we determined a resonance strength of $\omega\gamma_{251} = 482(82)$ µeV, in agreement with the literature value but with an improved relative uncertainty of 17% (previously 33% [16]) that is now comparable to that of the 309 keV resonance.

3.2. BGO detector phase: 140 keV resonance

During the search for the 140 keV resonance with the BGO de-tector, the 309 keV resonance was used as a reference to account
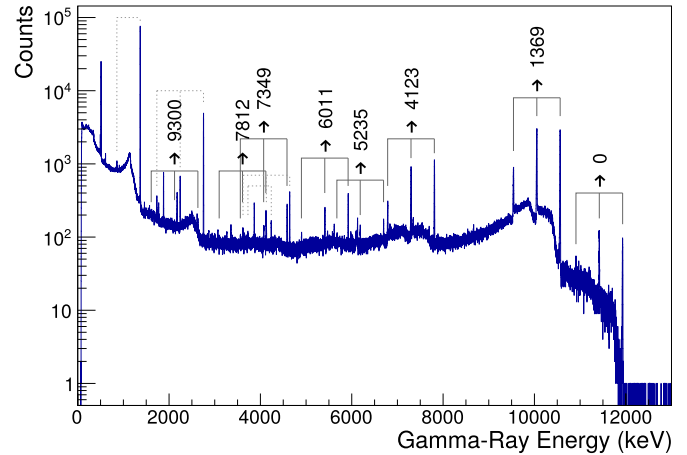

Fig. 3. HPGe spectrum acquired at $E_p = 255$ keV, $Q = 11.4$ C, indicating the major primary transitions from the 11931 keV state in ^{24}Mg. Dotted lines mark gamma rays and escape peaks from secondary transitions. The line at an energy corre-sponding to the ground state transition has been identified as caused purely by summing-in (see text for details).

Table 2
Branching ratios (in percent) for the state at $E_x = 11931$ keV in ^{24}Mg, populated through ^{23}Na(p, γ)^{24}Mg at $E_p = 251$ keV, to the levels E_f.

E_f (keV)	9300	8864	7812	7349	6011	5235	4238	4123	1369
[34]	–	–	–	–	–	–	–	11	89
this	0.14	0.25	1.05	1.21	3.21	0.95	0.38	18.2	74.6
work ±	0.05	0.05	0.12	0.14	0.34	0.16	0.14	1.8	7.5

for the influence of target composition variations on the yield. The yields Y and the strengths $\omega\gamma$ of the two resonances are related through $\frac{\omega\gamma_{140}}{\omega\gamma_{309}} = \frac{Y_{140}}{Y_{309}} \cdot \frac{\lambda^2_{309}}{\lambda^2_{140}} \cdot \frac{\varepsilon_{\text{eff},140}}{\varepsilon_{\text{eff},309}}$. Whilst the effective stopping power can vary considerably with changes in stoichiometry, the ratio of effective stopping powers at the two resonance energies is much more robust (with $< 1\%$ variation in this case).

We found two beam-induced backgrounds that were critical for the observation of the 140 keV resonance in our measure-ments: ^{7}Li(p, γ)^{8}Be with $Q = 17.25$ MeV, and ^{11}B(p, γ)^{12}C with $Q = 15.96$ MeV. With the Q-values of both background reac-tions larger than that of ^{23}Na(p, γ)^{24}Mg ($Q = 11.69$ MeV), these reactions can contribute to the ^{23}Na(p, γ)^{24}Mg region of inter-est (ROI) in the sum energy spectrum. The contribution of these backgrounds has been modeled as shown in Fig. 4. To illustrate the potential influence of these impurities, we compare the ex-pected yields: for a proton beam with an energy of 147 keV impinging on a 60 µg/cm^2 Na$_2$WO$_4$ target, the yield of a nar-row ^{23}Na(p, γ)^{24}Mg resonance with an $\omega\gamma$ at the current upper limit [9] is 15 reactions/C. The same reaction yield is obtained for ^{11}B(p, γ)^{12}C by a contamination of about 2500 ppm of boron, or for ^{7}Li(p,γ)^{8}Be by about 700 ppm of lithium.

Before and after each run in search of the 140 keV resonance, we scanned the 309 keV resonance to obtain a target profile and used the known gamma rays of the ^{23}Na(p, γ)^{24}Mg reaction to constrain the energy calibration of the individual detector seg-ments. Slightly non-linear energy responses from the detector seg-ments (especially at the higher gamma ray energies produced by the beam-induced backgrounds) were allowed by introducing a quadratic term in the energy calibration function. Using the energy calibrations of the individual crystals, we created the sum spec-trum.

Using the sum spectrum at energies above the total gamma-ray energy expected for the ^{23}Na(p, γ)^{24}Mg reaction, we obtained
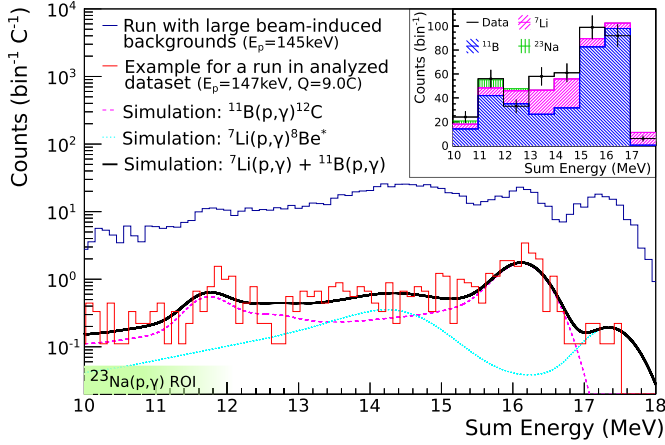
Fig. 4. Comparison of sum energy spectra for a target made from unfavorable raw material (large beam-induced background, blue) and an example of an analyzed spectrum taken with a cleaner target (red, 147 keV, 9.0 C). The modeled background contributions are shown to demonstrate the influence of ^{7}Li(p,γ)^{8}Be and ^{11}B(p,γ)^{12}C on the ^{23}Na(p, γ)^{24}Mg ROI. The inset shows the result (best fit) of a sum energy spectrum for one of the possible branching ratios of ^{23}Na(p, γ)^{24}Mg, with the binning used for the Bayesian analysis. See text for details.

constraints on the background-contributions from ^{7}Li and ^{11}B to the ^{23}Na(p, γ)^{24}Mg ROI. A Bayesian approach using Poisson-likelihood for the bin contents in this energy region (1 MeV wide bins between 10 MeV and 18 MeV) and uniform prior distributions for the yields of the background reactions results in a posterior probability distribution for the resonance strength, based on the excess of the number of counts in the ROI for the ^{23}Na(p, γ)^{24}Mg reaction over the contribution from the two beam-induced backgrounds (cf. inset of Fig. 4). The Bayesian Analysis Toolkit (BAT) [35] was used to calculate the posterior probability density function.

The relation between an excess over background in the ^{23}Na(p, γ)^{24}Mg reaction ROI and the ^{23}Na(p, γ)^{24}Mg reaction resonance strength requires knowledge of the detection efficiency, i.e., the probability of an ^{23}Na(p, γ)^{24}Mg event to cause a detected energy deposition in the corresponding ROI. This efficiency depends on the gamma-ray branchings, and spin and parity of the resonant level, which are unknown. We considered levels in ^{24}Mg with known branching ratios and E_x above 9 MeV, and simulated the corresponding detection efficiencies in the ROI around the respective E_x. This procedure corresponds to the approach in [9], except that all levels above 9 MeV were considered in this work, covering a wider range of possible branching ratios than the states selected in [9] and resulting in a larger detection efficiency uncertainty by comparison. Random sampling from the efficiencies corresponding to the branching ratios of different states was applied to include the effect of this uncertainty on the results for the resonance strength.

Different runs were performed within each chosen beam energy group. The posterior distributions for the resonance strength of the individual runs were combined to obtain a final posterior distribution. The posterior distribution obtained in the analysis for runs with 147 keV $\lesssim E_p \lesssim$ 149 keV is shown in Fig. 5. The posterior distribution has a mode at 1.46 neV, and the shortest interval to contain 68 % probability ranges from 0.94 and 2.05 neV (95 % interval from 0.51 to 2.74 neV).

4. Reaction rate and astrophysical implications

To summarize our results, the obtained strengths for the 309, 251 and 140 keV resonances are shown in Table 3. The value
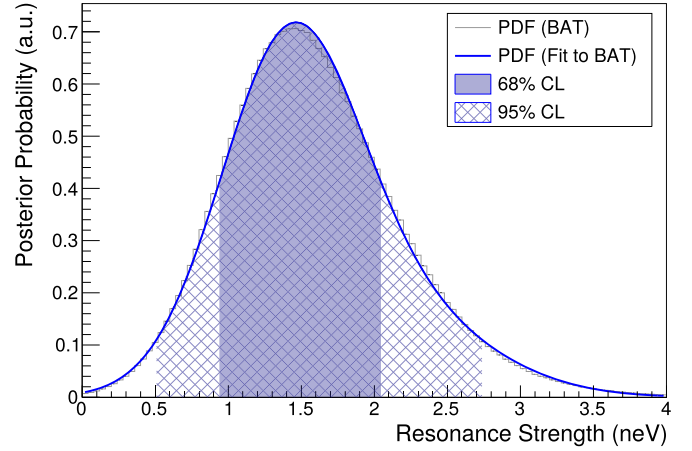

Fig. 5. Posterior probability density function for the strength of the 140 keV resonance.

Table 3
Resonance strengths for ^{23}Na(p, γ)^{24}Mg (in eV) of this work, compared to previous literature values. All uncertainties are given at 68% CL.

140 keV	251 keV	309 keV
[9]	[12,16]	[12,16]
$2.15(129) \times 10^{-9*}$	$5.25(175) \times 10^{-4}$	$1.05(19) \times 10^{-1}$
this work	this work	this work
$1.46^{+0.58}_{-0.53} \times 10^{-9}$	$4.82(82) \times 10^{-4}$	$1.08(19) \times 10^{-1}$

* When interpreting result of [9] as a positive detection; corresponds to an upper limit of < 5.17 neV at 95% CL otherwise.

for $\omega\gamma_{309}$ is in good agreement with the current literature value and has a comparable uncertainty. The $\omega\gamma_{251}$ has a reduced relative uncertainty of 17 % (previously: 33 % [16]). Moreover, we have found previously unobserved decay branches for the corresponding state in ^{24}Mg. We have directly observed the 140 keV resonance with an excess over zero of more than 2 σ for the first time. The new experimentally determined value for the strength of the 140 keV resonance is compatible with the result of [9] when interpreted as a positive detection, but we established it as a value different from zero with a much larger statistical significance and a relative uncertainty of 38 %.

With these results we calculated the ^{23}Na(p, γ)^{24}Mg reaction rate and determined its uncertainty by a Monte Carlo approach. Resonance strengths for $\omega\gamma_{309}$ and $\omega\gamma_{251}$ were sampled from Gaussian distributions, $\omega\gamma_{140}$ was sampled from the posterior distribution obtained in this measurement as discussed above. The direct capture strength and resonance energies were sampled as described in [11,10]. The resulting reaction rate, compared to the rates in [9], is shown in Fig. 6. The different treatment of the uncertainty of $\omega\gamma_{140}$ in this work and the upper limit in [9] should be noted for this comparison.

The relative uncertainty of the reaction rate is decreased in the temperature window $T = 0.05$–0.1 GK, thanks to the improved knowledge on the 140 keV resonance and the 251 keV resonance, with uncertainties between $^{+50\%}_{-35\%}$ at 0.07 GK and $^{+17\%}_{-14\%}$ at 0.1 GK. At $T = 0.06$–0.09 GK the reaction rate based on the results of this work is slightly higher than previously determined, because of the larger median value of $\omega\gamma_{140}$. Below $T = 0.05$ GK and above $T = 0.2$ GK, the reaction rate is dominated by the direct capture contribution and the 309 keV resonance (plus higher resonances), respectively, and is therefore unaffected by this work.

The main limiting factors for the determination of $\omega\gamma_{140}$ were the beam-induced backgrounds from traces of ^{7}Li and ^{11}B, the un-
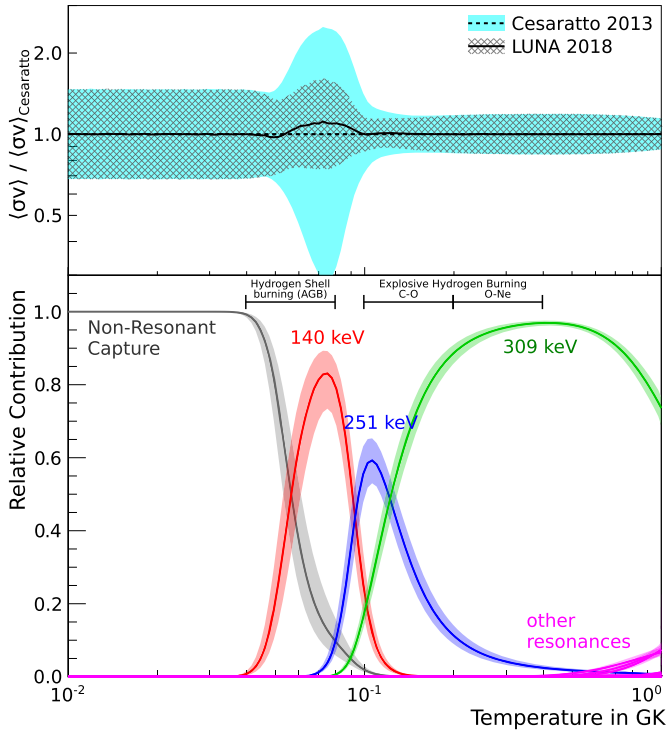
Fig. 6. Reaction rate and uncertainty (68% CL) based on the results presented in this work, compared to the reaction rate in [9]. Refer to the text for details on the different treatment of the uncertainty of the 140 keV resonance.
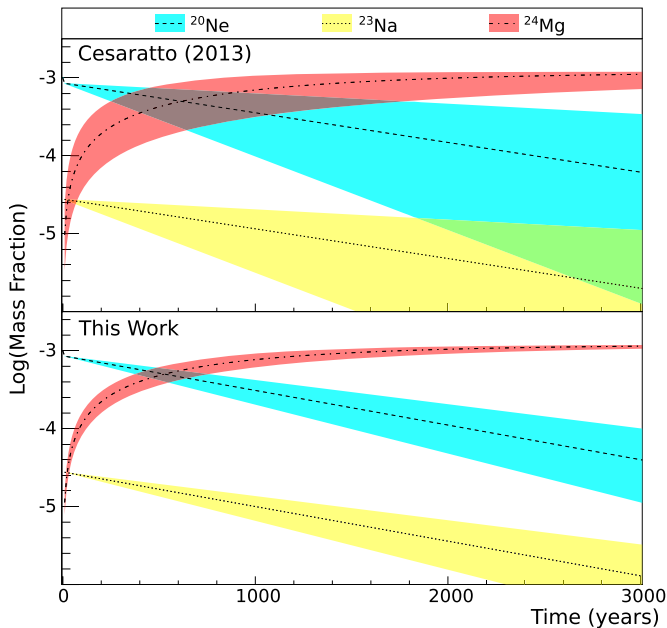

Fig. 7. Network calculations to follow ^{20}Ne, ^{23}Na and ^{24}Mg mass fractions, using the reaction rates of [9] (top) and this work (bottom) at T = 80 MK. See text for details.

certainty of the resonance energy, and the missing branching ratios for the resonant level.

To understand the potential impact of our results, we performed a network calculation for a constant $T = 80$ MK and $\rho = 10\,\mathrm{g/cm}^3$. The outcome of this calculation is shown in Fig. 7. The network includes all the isotopes of the NeNa cycle plus ^{24}Mg. The H and He mass fractions are kept constant, at $X(\mathrm{H}) = 0.5$ and $X(^4\mathrm{He}) = 0.499$, to simulate continuous replenishment via convec-

tion. The initial mass fractions of Ne and Na isotopes are scaled to solar abundances, with $X(\mathrm{Ne}) + X(\mathrm{Na}) = 0.001$, and initially $X(^{24}\mathrm{Mg}) = 0$. The calculations cover 3×10^3 yr, the typical time elapsed between two subsequent thermal pulses (instabilities of the He-burning shell) in an AGB star with initial mass $M = 7\,M_\odot$. Except for ^{22}Ne(p, γ)^{23}Na, reaction rates were taken from StarLib (version 6) [36], which includes the ^{23}Na(p, γ)^{24}Mg rates of [9]. For ^{22}Ne(p, γ)^{23}Na we used the most recent reaction rate from [8] (which is similar to the rate of [7]). The results of these calculations are shown in the upper panel of Fig. 7. The lower panel shows the results of the same calculation when using the ^{23}Na(p, γ)^{24}Mg rate based on this work.

The Ne and Na isotopes almost instantaneously reach their equilibrium abundances, and their abundance ratios, e.g. the ^{23}Na/^{20}Ne ratio, remain constant as they only depend on the temperature and the choice of the reaction rates. The continuous depletion of the total abundance of the Ne and Na isotopes is driven by the leakage of the ^{23}Na(p, γ)^{24}Mg reaction. As a consequence the ^{24}Mg piles up. The shaded areas in Fig. 7 represent the influence of the ^{23}Na(p, γ)^{24}Mg reaction rate on the three most abundant Ne, Na, and Mg isotopes during this nucleosynthesis episode. The reduction of the uncertainties when passing from the previous [9] and the new rate is evident. This result will improve future calculations of the yields of massive AGB stars, providing, in particular, a more accurate understanding of the evolution of the Na and Mg isotopes in galaxies and stellar clusters.

Acknowledgements

References

[1] M. Forestini, C. Charbonnel, Nucleosynthesis of light elements inside thermally pulsing AGB stars: I. The case of intermediate-mass stars, Astron. Astrophys. Suppl. Ser. 123 (1997) 241–272, https://doi.org/10.1051/aas:1997348, arXiv:astro-ph/9608153.

[2] J.C. Lattanzio, C.A. Frost, R.C. Cannon, P.R. Wood, Hot bottom burning nucleosynthesis in 6 M$_\odot$ stellar models, Nucl. Phys. A 621 (1997) 435–438, https://doi.org/10.1016/S0375-9474(97)00286-8.

[3] R.G. Izzard, M. Lugaro, A.I. Karakas, C. Iliadis, M. van Raai, Reaction rate uncertainties and the operation of the NeNa and MgAl chains during HBB in intermediate-mass AGB stars, Astron. Astrophys. 466 (2) (2007) 641–648, https://doi.org/10.1051/0004-6361:20066903.

[4] F. Cavanna, R. Depalo, M. Aliotta, M. Anders, D. Bemmerer, A. Best, A. Boeltzig, C. Broggini, C.G. Bruno, A. Caciolli, P. Corvisiero, T. Davinson, A. di Leva, Z. Elekes, F. Ferraro, A. Formicola, Z. Fülöp, G. Gervino, A. Guglielmetti, C. Gustavino, G. Gyürky, G. Imbriani, M. Junker, R. Menegazzo, V. Mossa, F.R. Pantaleo, P. Prati, D.A. Scott, E. Somorjai, O. Straniero, F. Strieder, T. Szücs, M.P. Takács, D. Trezzi, The LUNA Collaboration, Three new low-energy resonances in the ^{22}Ne(p,γ)^{23}Na reaction, Phys. Rev. Lett. 115 (25) (2015), https://doi.org/10.1103/PhysRevLett.115.252501.

[5] F. Cavanna, R. Depalo, M. Aliotta, M. Anders, D. Bemmerer, A. Best, A. Boeltzig, C. Broggini, C.G. Bruno, A. Caciolli, P. Corvisiero, T. Davinson, A. di Leva, Z. Elekes, F. Ferraro, A. Formicola, Z. Fülöp, G. Gervino, A. Guglielmetti, C. Gustavino, G. Gyürky, G. Imbriani, M. Junker, R. Menegazzo, V. Mossa, F.R. Pantaleo, P. Prati, D.A. Scott, E. Somorjai, O. Straniero, F. Strieder, T. Szücs, M.P. Takács,

D. Trezzi, The LUNA Collaboration, Erratum: Three new low-energy resonances in the ^{22}Ne(p,γ)^{23}Na reaction [Phys. Rev. Lett. 115 (2015) 252501], Phys. Rev. Lett. 120 (23) (2018) 239901, https://doi.org/10.1103/PhysRevLett.120.239901.

[6] R. Depalo, F. Cavanna, M. Aliotta, M. Anders, D. Bemmerer, A. Best, A. Boeltzig, C. Broggini, C.G. Bruno, A. Cacioli, G.F. Ciani, P. Corvisiero, T. Davinson, A. Di Leva, Z. Elekes, F. Ferraro, A. Formicola, Z. Fülöp, G. Gervino, A. Guglielmetti, C. Gustavino, G. Gyürky, G. Imbriani, M. Junker, R. Menegazzo, V. Mossa, F.R. Pantaleo, D. Piatti, P. Prati, O. Straniero, T. Szücs, M.P. Takács, D. Trezzi, LUNA Collaboration, Direct measurement of low-energy ^{22}Ne(p,γ)^{23}Na resonances, Phys. Rev. C 94 (5) (2016), https://doi.org/10.1103/PhysRevC.94.055804.

[7] K.J. Kelly, A.E. Champagne, L.N. Downen, J.R. Dermigny, S. Hunt, C. Iliadis, A.L. Cooper, New measurements of low-energy resonances in the ^{22}Ne(p,γ)^{23}Na reaction, Phys. Rev. C 95 (1) (2017) 015806, https://doi.org/10.1103/PhysRevC.95.015806.

[8] F. Ferraro, M.P. Takács, D. Piatti, F. Cavanna, R. Depalo, M. Aliotta, D. Bemmerer, A. Best, A. Boeltzig, C. Broggini, C.G. Bruno, A. Cacioli, T. Chillery, G.F. Ciani, P. Corvisiero, T. Davinson, G. D'Erasmo, A. Di Leva, Z. Elekes, E.M. Fiore, A. Formicola, Z. Fülöp, G. Gervino, A. Guglielmetti, C. Gustavino, G. Gyürky, G. Imbriani, M. Junker, A. Karakas, I. Kochanek, M. Lugaro, P. Marigo, R. Menegazzo, V. Mossa, F.R. Pantaleo, V. Paticchio, R. Perrino, P. Prati, L. Schiavulli, K. Stöckel, O. Straniero, T. Szücs, D. Trezzi, S. Zavatarelli, LUNA Collaboration, Direct capture cross section and the Ep = 71 and 105 keV resonances in the ^{22}Ne(p,γ)^{23}Na reaction, Phys. Rev. Lett. 121 (17) (2018) 172701, https://doi.org/10.1103/PhysRevLett.121.172701.

[9] J.M. Cesaratto, A.E. Champagne, M.Q. Buckner, T.B. Clegg, S. Daigle, C. Howard, C. Iliadis, R. Longland, J.R. Newton, B.M. Oginni, Measurement of the $E_r^{c.m.} = 138$ keV resonance in the ^{23}Na(p,γ)^{24}Mg reaction and the abundance of sodium in AGB stars, Phys. Rev. C 88 (6) (2013) 065806, https://doi.org/10.1103/PhysRevC.88.065806.

[10] C. Iliadis, R. Longland, A. Champagne, A. Coc, Charged-particle thermonuclear reaction rates: III. Nuclear physics input, Nucl. Phys. A 841 (1–4) (2010) 251–322, https://doi.org/10.1016/j.nuclphysa.2010.04.010.

[11] R. Longland, C. Iliadis, A. Champagne, J. Newton, C. Ugalde, A. Coc, R. Fitzgerald, Charged-particle thermonuclear reaction rates: I. Monte Carlo method and statistical distributions, Nucl. Phys. A 841 (1–4) (2010) 1–30, https://doi.org/10.1016/j.nuclphysa.2010.04.008.

[12] Z. Switkowski, R. O'Brien, A. Smith, D. Sargood, Total yield measurements in ^{23}Na(p,γ)^{24}Mg, Aust. J. Phys. 28 (2) (1975) 141, https://doi.org/10.1071/PH750141.

[13] B.M. Paine, S.R. Kennett, D.G. Sargood, (p,γ) resonance strengths in the s-d shell, Phys. Rev. C 17 (5) (1978) 1550–1554, https://doi.org/10.1103/PhysRevC.17.1550.

[14] B. Paine, D. Sargood, (p,γ) Resonance strengths in the s-d shell, Nucl. Phys. A 331 (2) (1979) 389–400, https://doi.org/10.1016/0375-9474(79)90349-X.

[15] J. Görres, M. Wiescher, C. Rolfs, Hydrogen burning of ^{23}Na in the NeNa cycle, Astrophys. J. 343 (1989) 365, https://doi.org/10.1086/167710.

[16] P. Endt, Energy levels of A = 21-44 nuclei (VII), Nucl. Phys. A 521 (1990) 1–400, https://doi.org/10.1016/0375-9474(90)90598-G.

[17] S. Hale, A. Champagne, C. Iliadis, V. Hansper, D. Powell, J. Blackmon, Investigation of the ^{23}Na(p,γ)^{24}Mg and ^{23}Na(p,α)^{20}Ne reactions via (^{3}He,d) spectroscopy, Phys. Rev. C 70 (4) (2004) 045802, https://doi.org/10.1103/PhysRevC.70.045802.

[18] National Nuclear Data Center, information extracted from the NuDat 2 database, http://www.nndc.bnl.gov/nudat2/, 2017.

[19] R. Firestone, Nuclear data sheets for A = 24, Nucl. Data Sheets 108 (11) (2007) 2319–2392, https://doi.org/10.1016/j.nds.2007.10.001.

[20] S. Wagner, M. Heitzmann, Resonanzenergien für den Protoneneinfang II. Natrium, Z. Naturforsch. A 15 (1) (1960), https://doi.org/10.1515/zna-1960-0111.

[21] S. Wüstenbecker, H. Ebbing, W. Schulte, H. Baumeister, H. Becker, B. Cleff, C. Rolfs, H. Trautvetter, G. Mitchell, J. Schweitzer, C. Peterson, Improvements in targetry and high voltage stability for high resolution ion beam experiments, Nucl. Instrum. Methods Phys. Res., Sect. A, Accel. Spectrom. Detect. Assoc. Equip. 279 (3) (1989) 448–466, https://doi.org/10.1016/0168-9002(89)91292-8.

[22] A. Formicola, G. Imbriani, M. Junker, D. Bemmerer, R. Bonetti, C. Broggini, C. Casella, P. Corvisiero, H. Costantini, G. Gervino, C. Gustavino, A. Lemut, P. Prati, V. Roca, C. Rolfs, M. Romano, D. Schürmann, F. Strieder, H.-P. Trautvetter, S. Zavatarelli, The LUNA II 400 kV accelerator, Nucl. Instrum. Methods Phys. Res., Sect. A, Accel. Spectrom. Detect. Assoc. Equip. 507 (3) (2003) 609–616, https://doi.org/10.1016/S0168-9002(03)01435-9.

[23] H. Costantini, A. Formicola, G. Imbriani, M. Junker, C. Rolfs, F. Strieder, LUNA: a laboratory for underground nuclear astrophysics, Rep. Prog. Phys. 72 (8) (2009) 086301, https://doi.org/10.1088/0034-4885/72/8/086301.

[24] D. Bemmerer, F. Confortola, A. Lemut, R. Bonetti, C. Broggini, P. Corvisiero, H. Costantini, J. Cruz, A. Formicola, Z. Fülöp, G. Gervino, A. Guglielmetti, C. Gustavino, G. Gyürky, G. Imbriani, A.P. Jesus, M. Junker, B. Limata, R. Menegazzo,

P. Prati, V. Roca, D. Rogalla, C. Rolfs, M. Romano, C. Rossi Alvarez, F. Schümann, E. Somorjai, O. Straniero, F. Strieder, F. Terrasi, H.P. Trautvetter, A. Vomiero, Feasibility of low-energy radiative-capture experiments at the LUNA underground accelerator facility, Eur. Phys. J. A 24 (2) (2005) 313–319, https://doi.org/10.1140/epja/i2004-10135-4.

[25] A. Boeltzig, A. Best, G. Imbriani, M. Junker, M. Aliotta, D. Bemmerer, C. Broggini, C.G. Bruno, R. Buompane, A. Cacioli, F. Cavanna, T. Chillery, G.F. Ciani, P. Corvisiero, L. Csedreki, T. Davinson, R.J. deBoer, A. Di Leva, Z. Elekes, F. Ferraro, E.M. Fiore, A. Formicola, Z. Fülöp, G. Gervino, A. Guglielmetti, C. Gustavino, G. Gyürky, I. Kochanek, R. Menegazzo, V. Mossa, F.R. Pantaleo, V. Paticchio, R. Perrino, D. Piatti, P. Prati, L. Schiavulli, K. Stöckel, O. Straniero, F. Strieder, T. Szücs, M.P. Takács, D. Trezzi, M. Wiescher, S. Zavatarelli, Improved background suppression for radiative capture reactions at LUNA with HPGe and BGO detectors, J. Phys. G, Nucl. Part. Phys. 45 (2) (2018) 025203, https://doi.org/10.1088/1361-6471/aaa163.

[26] F. Strieder, B. Limata, A. Formicola, G. Imbriani, M. Junker, D. Bemmerer, A. Best, C. Broggini, A. Cacioli, P. Corvisiero, H. Costantini, A. DiLeva, Z. Elekes, Z. Fülöp, G. Gervino, A. Guglielmetti, C. Gustavino, G. Gyürky, A. Lemut, M. Marta, C. Mazzocchi, R. Menegazzo, P. Prati, V. Roca, C. Rolfs, C. Rossi Alvarez, E. Somorjai, O. Straniero, F. Terrasi, H. Trautvetter, The ^{25}Mg(p, γ)^{26}Al reaction at low astrophysical energies, Phys. Lett. B 707 (1) (2012) 60–65, https://doi.org/10.1016/j.physletb.2011.12.029.

[27] J. Allison, K. Amako, J. Apostolakis, P. Arce, M. Asai, T. Aso, E. Bagli, A. Bagulya, S. Banerjee, G. Barrand, B. Beck, A. Bogdanov, D. Brandt, J. Brown, H. Burkhardt, P. Canal, D. Cano-Ott, S. Chauvie, K. Cho, G. Cirrone, G. Cooperman, M. Cortés-Giraldo, G. Cosmo, G. Cuttone, G. Depaola, L. Desorgher, X. Dong, A. Dotti, V. Elvira, G. Folger, Z. Francis, A. Galoyan, L. Garnier, M. Gayer, K. Genser, V. Grichine, S. Guatelli, P. Guèye, P. Gumplinger, A. Howard, I. Hřivnáčová, S. Hwang, S. Incerti, A. Ivanchenko, V. Ivanchenko, F. Jones, S. Jun, P. Kaitaniemi, N. Karakatsanis, M. Karamitros, M. Kelsey, A. Kimura, T. Koi, H. Kurashige, A. Lechner, S. Lee, F. Longo, M. Maire, D. Mancusi, A. Mantero, E. Mendoza, B. Morgan, K. Murakami, T. Nikitina, L. Pandola, P. Paprocki, J. Perl, I. Petrović, M. Pia, W. Pokorski, J. Quesada, M. Raine, M. Reis, A. Ribon, A. Ristić Fira, F. Romano, G. Russo, G. Santin, T. Sasaki, D. Sawkey, J. Shin, I. Strakovsky, A. Taborda, S. Tanaka, B. Tomé, T. Toshito, H. Tran, P. Truscott, L. Urban, V. Uzhinsky, J. Verbeke, M. Verderi, B. Wendt, H. Wenzel, D. Wright, D. Wright, T. Yamashita, J. Yarba, H. Yoshida, Recent developments in Geant 4, Nucl. Instrum. Methods Phys. Res., Sect. A, Accel. Spectrom. Detect. Assoc. Equip. 835 (2016) 186–225, https://doi.org/10.1016/j.nima.2016.06.125.

[28] A. Di Leva, D.A. Scott, A. Cacioli, A. Formicola, F. Strieder, M. Aliotta, M. Anders, D. Bemmerer, C. Broggini, P. Corvisiero, Z. Elekes, Z. Fülöp, G. Gervino, A. Guglielmetti, C. Gustavino, G. Gyürky, G. Imbriani, J. José, M. Junker, M. Laubenstein, R. Menegazzo, E. Napolitani, P. Prati, V. Rigato, V. Roca, E. Somorjai, C. Salvo, O. Straniero, T. Szücs, F. Terrasi, D. Trezzi, Underground study of the ^{17}O(p,γ)^{18}F reaction relevant for explosive hydrogen burning, Phys. Rev. C 89 (1) (2014), https://doi.org/10.1103/PhysRevC.89.015803.

[29] G. Imbriani, H. Costantini, A. Formicola, A. Vomiero, C. Angulo, D. Bemmerer, R. Bonetti, C. Broggini, F. Confortola, P. Corvisiero, J. Cruz, P. Descouvemont, Z. Fülöp, G. Gervino, A. Guglielmetti, C. Gustavino, G. Gyürky, A.P. Jesus, M. Junker, J.N. Klug, A. Lemut, R. Menegazzo, P. Prati, V. Roca, C. Rolfs, M. Romano, C. Rossi-Alvarez, F. Schümann, E. Somorjai, O. Straniero, F. Strieder, F. Terrasi, H.P. Trautvetter, S-factor of ^{14}N(p,γ)^{15}O at astrophysical energies, Eur. Phys. J. A 25 (3) (2005) 455–466, https://doi.org/10.1140/epja/i2005-10138-7.

[30] U. Kreissig, S. Grigull, K. Lange, P. Nitzsche, B. Schmidt, In situ ERDA studies of ion drift processes during anodic bonding of alkali-borosilicate glass to metal, Nucl. Instrum. Methods Phys. Res., Sect. B, Beam Interact. Mater. Atoms 136–138 (1998) 674–679, https://doi.org/10.1016/S0168-583X(97)00778-7.

[31] N.P. Barradas, C. Jeynes, R.P. Webb, Simulated annealing analysis of Rutherford backscattering data, Appl. Phys. Lett. 71 (2) (1997) 291–293, https://doi.org/10.1063/1.119524.

[32] C.E. Rolfs, W.S. Rodney, Cauldrons in the Cosmos: Nuclear Astrophysics, Theoretical Astrophysics, University of Chicago Press, Chicago, 1988.

[33] J.F. Ziegler, SRIM 2013, http://srim.org.

[34] J. L'Ecuyer, R.J.A. Lévesque, La réaction ^{23}Na(p,γ)^{24}Mg pour des protons d'énergie inférieure à 500 keV, Can. J. Phys. 44 (10) (1966) 2201–2210, https://doi.org/10.1139/p66-178.

[35] A. Caldwell, D. Kollár, K. Kröninger, BAT – The Bayesian analysis toolkit, Comput. Phys. Commun. 180 (11) (2009) 2197–2209, https://doi.org/10.1016/j.cpc.2009.06.026.

[36] A.L. Sallaska, C. Iliadis, A.E. Champagne, S. Goriely, S. Starrfield, F.X. Timmes, STARLIB: a next-generation reaction-rate library for nuclear astrophysics, Astrophys. J. Suppl. Ser. 207 (1) (2013) 18, https://doi.org/10.1088/0067-0049/207/1/18.